ADVANCED MATERIALS
www.advmat.de

Spiro-Phenothiazine Hole-Transporting Materials: Unlocking Stability and Scalability in Perovskite Solar Cells

Javier Urieta-Mora, Seung Ju Choi, Jaeki Jeong, Silvia Orecchio, Inés García-Benito, Manuel Pérez-Escribano, Joaquín Calbo, Likai Zheng, Minseop Byun, Seyeong Song, Gi-Hwan Kim, Shaik M. Zakeeruddin, Seog-Young Yoon, Yimhyun Jo, Agustín Molina-Ontoria,* Enrique Ortí,* Nazario Martín,* and Michael Grätzel**

Improving both the efficiency and long-term stability of perovskite solar cells (PSCs) is critical for their commercial deployment. Despite the widespread use of spiro-OMeTAD as a hole-transporting material (HTM), its inhomogeneous doping behavior and susceptibility to moisture and heat have hindered its large-scale industrial implementation. Here, a family of spiro-phenothiazine-based HTMs (PTZ) is reported to address these drawbacks. Among them, the fluorene derivative (PTZ-Fl) shows a larger Li^+ affinity and forms a compact interphase by intercalation in the perovskite passivating layer that prevents Li^+ migration. PSCs incorporating PTZ-Fl exhibit power conversion efficiencies (PCEs) up to 25.8% (certified 25.2% under reverse scan), retaining 80% of their initial performance after 1000 h under ISOS-L-3 protocol. Furthermore, a 5 × 5 cm mini-module reaches a PCE of 22.1%, surpassing spiro-OMeTAD-based PSCs and retaining over 85% of its efficiency after 1100 h under ISOS-D-1 protocol. These results demonstrate that PTZ-Fl not only enables high PCEs but also substantially improves operational stability, offering a promising pathway toward the large-scale deployment of next-generation PSCs.

1. Introduction

Since the seminal report of Miyasaka in 2009 on the use of perovskite materials for solar energy applications,[1] the scientific community has been attracted by the unprecedented development of this groundbreaking technology, reaching, in a decade of research, power conversion efficiencies (PCEs) up to 27%, similar to those exhibited by monocrystalline silicon technologies.[2–7] The appealing optoelectronic properties and low-cost fabrication ofPSCs motivate the development of this new technology, but important improvements concerning the device stability are still necessary for its commercial application.[8] One of the reasons causing the low stability of PSCs is attributed to the presence of under-coordinated lead ions in hybrid organic–inorganic perovskite materials, which

J. Urieta-Mora, S. Orecchio, I. García-Benito, A. Molina-Ontoria, N. Martín
Departamento Química Orgánica
Facultad C. C. Químicas
Universidad Complutense de Madrid
Av. Complutense s/n, Madrid 28040, Spain
E-mail: amolinao@ucm.es; nazmar@ucm.es

J. Urieta-Mora, N. Martín
IMDEA-Nanociencia
C/ Faraday 9
Ciudad Universitaria de Cantoblanco
Madrid 28049, Spain

The ORCID identification number(s) for the author(s) of this article can be found under https://doi.org/10.1002/adma.202505475

[Correction added on August 8, 2025, after first online publication: Affiliation of Y.J. was updated.]

DOI: 10.1002/adma.202505475

S. J. Choi, M. Byun, Y. Jo
Ulsan Advanced Energy Technology R&D Center
Korea Institute of Energy Research
25 Techno Saneop-ro 55beon-gil, Nam-gu, Ulsan 44776, Republic of Korea
E-mail: yimhyun.jo@kier.re.kr

S. J. Choi, S.-Y. Yoon
School of Materials Science and Engineering
Pusan National University
Busan 46241, Republic of Korea

J. Jeong, L. Zheng, S. M. Zakeeruddin, M. Grätzel
Laboratory of Photonics and Interfaces
Institute of Chemical Sciences and Engineering
École Polytechnique Fédérale de Lausanne (EPFL)
Lausanne CH-1015, Switzerland
E-mail: michael.graetzel@epfl.ch

J. Jeong
Department of Energy Science
Sungkyunkwan University
2066 Seoburo, Suwon 35017, Republic of Korea

S. Orecchio
Department of Biological
Chemical and Pharmaceutical Sciences and Technologies University of Palermo
Viale delle Scienze s/n Ed. 17, Palermo 90128, Italy

causes the formation of defect states within the bandgap where the free carriers are trapped, thereby not only reducing the efficiency of the devices but also promoting the degradation of the material due to the charge accumulation at these defects.[9,10]

One of the methods to improve device stability is through the surface passivation of the perovskite. Thus, the HTMs) can be employed not only as a charge carrier selective contact but also as a protective layer of the photoactive perovskite material against ambient conditions such as moisture.[11] The chemical optimization of hole-transporting materials has been widely studied in PSCs. In this regard, different structures such as inorganic compounds,[12,13] polymeric structures,[14,15] and small organic molecules have been reported during the last decade.[16,17] Organic small-molecule HTMs are appealing structures due to their structural chemical versatility, simple synthesis and purification, and tailored optoelectronic properties. Among them, spiro-containing central scaffolds, such as the well-known 2,2′,7,7′-tetrakis-(*N*,*N*-di-4-methoxyphenylamino)-9,9′-spirobifluorene, commonly known as spiro-OMeTAD, have been successfully used for achieving highly efficient PSCs, which is mainly attributed to their excellent ability to form smooth films.[18] Despite its widespread use, spiro-OMeTAD suffers from limited thermal and environmental stability, which hampers its suitability for long-term operation and large-scale applications, in addition to its complex synthesis. Alternative spiran-type structures have been recently reported, demonstrating the potential of spiro-based molecules.[19–21] Other small organic molecules reported in the bibliography as efficient HTMs include extended polycyclic aromatic hydrocarbons (PAHs)[22–27] and donor-acceptor systems.[28,29]

Herein, we report four new HTMs using spiro-phenothiazine central scaffold, extended by peripheral arylamine units modified by the asymmetric introduction of different aromatic fragments, such as naphthyl or fluorene, or the substitution by fluorine atoms (**Figure 1a**). In a previous study, we demonstrated that incorporating phenoxazine and phenothiazine units in a spiro-like structure afforded efficiencies comparable to the benchmark spiro-OMeTAD, while significantly improving the long-term stability.[21] The new chemical design proposed in this work modifies the optoelectronic and thermal properties of the spiro-phenothiazine materials. The new HTMs were incorporated into planar n-i-p devices using Cl-modified $FAPbI_3$, in combination with a 2D interface featuring 4-methoxy-phenethylammonium iodide (m-PEAI), leading to PCEs in PSCs of up to 25.8%. Additionally, the device incorporating the fluorene-derivatized compound (PTZ-Fl) as HTM retained 80% of its initial efficiency after 1000 h under maximum power point tracking, as specified by the ISOS-L-3 test protocol. Furthermore, we successfully scaled up the PTZ-Fl-based perovskite module (25 cm^2) with a PCE of 22.07%, which retained 85% of its initial efficiency for 1100 h.

2. Results and Discussion

2.1. Structural, Optoelectronic and Thermal Properties of PTZ HTMs

The synthesis of the new PTZ derivatives was approached following the previous reported procedure (experimental details are included in the Supporting Information).[21] The estimated synthetic costs for the preparation of the new HTMs are calculated in the range of 47–75 € g^{-1} (see Table S10, Supporting Information for further details). Complete structural characterization of the four new spiro-based HTMs was carried out using standard spectroscopic analysis such as NMR (^1H and ^{13}C), Fourier-transform infrared spectroscopy (FTIR), and mass spectrometry. The high-resolution MALDI-TOF analysis confirmed the formation of the tailored HTMs, exhibiting the respective molecular ion peaks (see Figures S33, S36, S40, and S44, Supporting Information). Figure 1b shows an energy band diagram of the perovskite and the HTMs.

Relevant insights into the thermal properties of the new HTMs were provided by thermogravimetric analysis (TGA) and differential scanning calorimetry (DSC). The TGA curves shown in Figure 1c confirm good thermal stability with decomposition temperatures (T_{dec}) higher than 350 °C (Table S1, Supporting Information). However, the T_{dec} values recorded for the asymmetric HTMs are significantly lower, especially for those bearing fluorine atoms, than the T_{dec} of spiro-OMeTAD (449 °C). DSC thermograms (Figure 1d) reveal that the PTZ-based HTMs present a similar morphological behavior, exhibiting glass transition temperatures (T_g) of 175, 187, 152, and 142 °C for PTZ-NaPh, PTZ-Fl, PTZ-3F, and PTZ-4F, respectively. Interestingly, these T_g values are higher than those measured for spiro-OMeTAD (125 °C), indicating a reduced tendency to crystallize. This can contribute to enhancing the long-term thermal stability of the resultant devices. After consecutive heating/cooling cycles, only small changes in the T_g were observed.

To characterize the influence of the PTZ-based HTMs on the surface crystalline properties of the perovskite films, grazing-incidence wide-angle X-ray scattering (GIWAXS) measurements were conducted (Figure 1e; Figure S11, Supporting Information). The out-of-plane patterns with low q_z values (less than 0.7 $Å^{-1}$) can be attributed to lamellar molecular ordering of HTMs, as evidenced by (n00) reflections (where "n00" denotes reflections arising from planes oriented parallel to the substrate). The q_z values gradually decrease in the order of 0.314 $Å^{-1}$ (Control) > 0.312 $Å^{-1}$ (PTZ-Fl) > 0.311 $Å^{-1}$ (PTZ-3F) > 0.310 $Å^{-1}$ (PTZ-4F), indicating that an increasing number of fluorine substituents leads

I. García-Benito
COMET-NANO Group
Department of Biology and Geology
Physics and Inorganic Chemistry
ESCET
Universidad Rey Juan Carlos
Calle Tulipán s/n, Móstoles E-28933, Spain
M. Pérez-Escribano, J. Calbo, E. Ortí
Instituto de Ciencia Molecular
Universidad de Valencia
Catedrático José Beltrán 2, Paterna 46980, Spain
E-mail: enrique.orti@uv.es
S. Song
School of Energy and Chemical Engineering
Ulsan National Institute of Science and Technology (UNIST)
Ulsan 44919, South Korea
S. Song, G.-H. Kim
Department of Materials Engineering and Convergence Technology
Gyeongsang National University
Jinju 52828, Republic of Korea

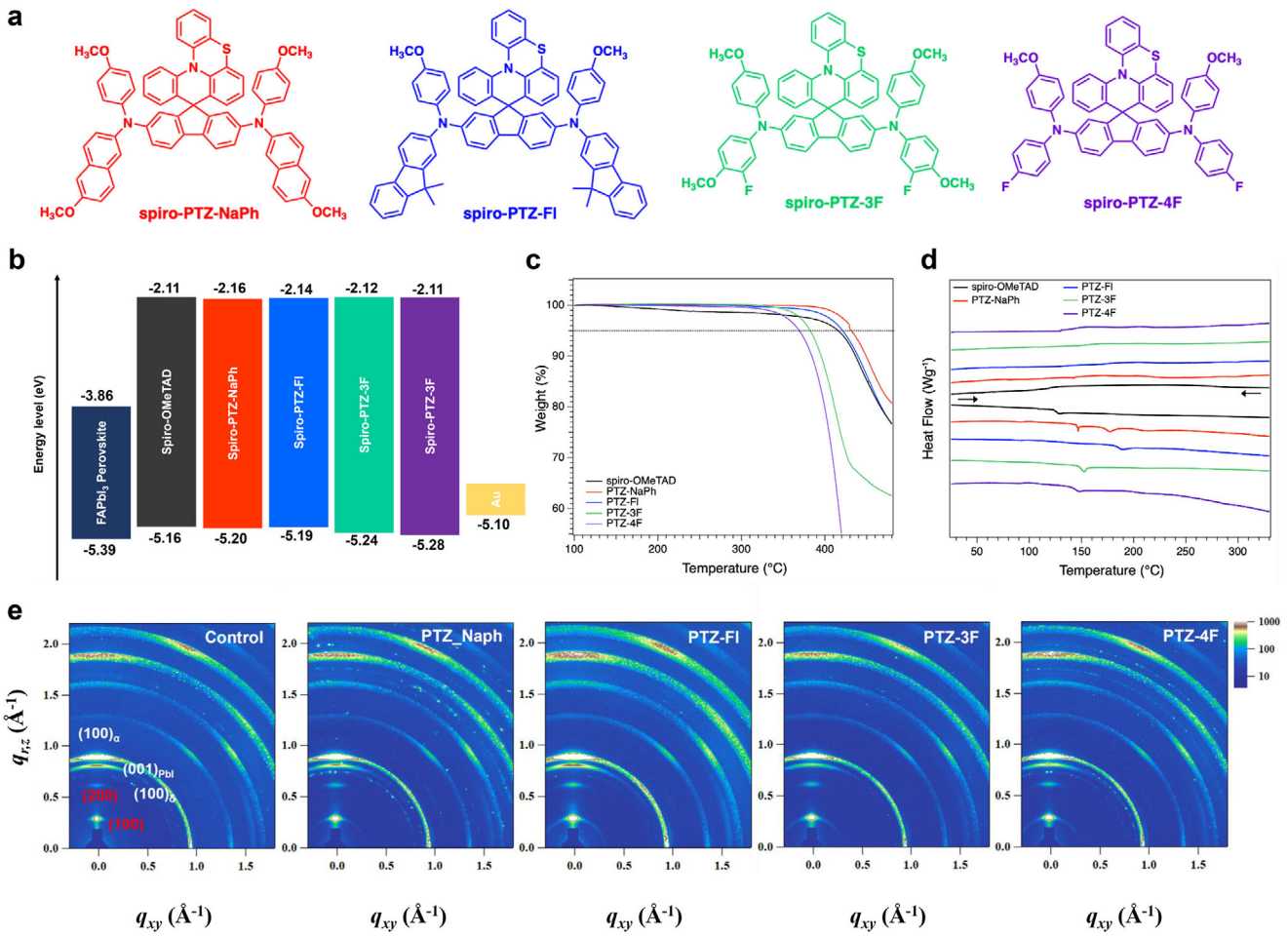

Figure 1. a) Chemical structure of the new asymmetric PTZ-based HTMs. b) Energy levels of the perovskite and the spiro-OMeTAD and PTZ-based HTMs. c) TGA of the PTZ-based HTMs under nitrogen at 10 °C min^{-1} heating rate. d) DSC curves recorded for the PTZ-based HTMs under nitrogen at a heating rate of 20 °C min^{-1} (second cycle). e) 2D GIWAXS scattering patterns in q space for perovskite film with control and PTZ-based HTMs.

to larger lamellar d-spacings. Notably, PTZ-Fl exhibits stronger lamellar diffraction intensity with a predominantly edge-on orientation. On the other hand, the perovskite q value of ring patterns in 2D GIWAXS spectra for the PTZ-Fl film shows substantially higher out-of-plane diffraction intensity, which suggests enhanced perovskite crystallinity. Furthermore, the results for the control, PTZ-Naph, and PTZ-4F samples clearly reveal the presence of a δ-phase diffraction peak at $q_z = 0.8$ $Å^{-1}$, whereas this phase is nearly negligible in the PTZ-Fl and PTZ-3F films.

DFT calculations predict minimum-energy molecular structures for the PTZ-HTMs in which the spiro-phenothiazine scaffold shows π–π interactions with one of the aromatic substituents of the peripheral arylamine units, with contacts in the range from 3.5 to 4.7 Å (see Figure S1a and full computational details in the Supporting Information). This interaction, which is displayed in **Figure** 2a for PTZ-Fl, provides an electron-dense region that promotes the binding of Li^+, effectively reducing its migration within the HTM layer when doped with Li-TFSI (vide infra).

The optical properties of the new family of spiro-PTZ compounds were evaluated and compared to those of spiro-OMeTAD using UV–vis absorption and fluorescence experiments in CH_2Cl_2 solution (see Figure 2b). The optical characteristics are summarized in Table S1 (Supporting Information). PTZ-NaPh and PTZ-Fl exhibit a broader and slightly redshifted absorption band due to the extended π-conjugation through the peripheral naphthalene and fluorene units, respectively, when compared with the peripheral p-anisole moieties in spiro-OMeTAD, PTZ-3F, and PTZ-4F. Time-dependent DFT (TD-DFT) calculations predict that, in all cases, the lowest-energy absorption band corresponds to the $S_0 \rightarrow S_1$ electronic transition calculated at ≈400 nm, which is mainly described by the HOMO→LUMO mono-excitation involving the central fluorene and the arylamine units (Figure S1b, Supporting Information). Regarding the emission spectra (Figure 2b), a broad band is observed starting at ≈400 nm giving rise to low Stokes shifts, as also observed for spiro-OMeTAD.

The electron donor character of the new spiro-PTZ-based HTMs was evaluated using cyclic voltammetry measurements in CH_2Cl_2 solutions containing 0.1 M of $TBAPF_6$, which acts as the supporting electrolyte, at a scan rate of 100 mV s^{-1} (Figure 2c). Table S1 (Supporting Information) summarizes the redox potential of the PTZ HTMs, including the HOMO energies estimated

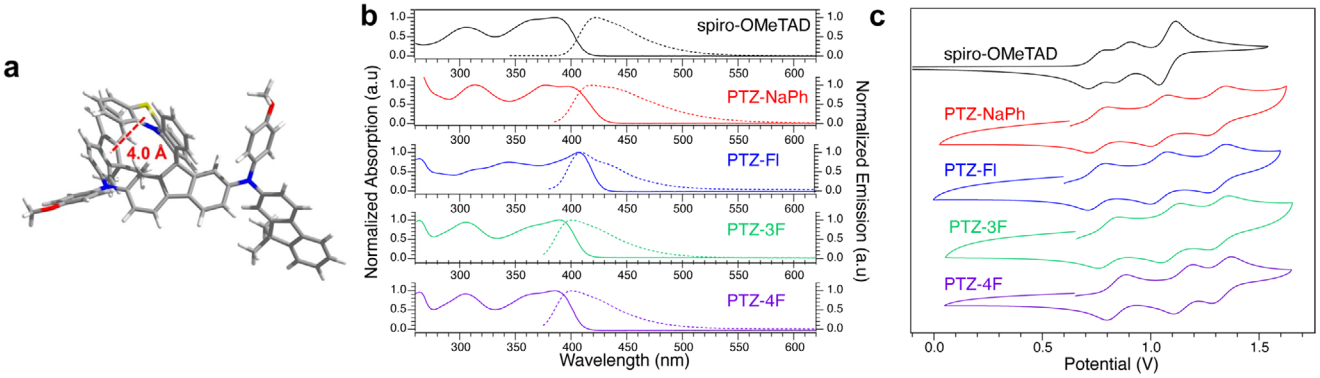

Figure 2. a) BMK/6-31G(d,p)+PCM minimum-energy structure calculated for PTZ-FI. Atom color code: C (gray), S (yellow), N (blue), O (red) and H (white). b) UV–vis absorption spectra (solid line) and emission spectra (dashed line) recorded for the new PTZ HTMs and spiro-OMeTAD (CH_2Cl_2 solution, 10^{-6} M). c) Cyclic voltammograms recorded for the new PTZ HTMs and spiro-OMeTAD in CH_2Cl_2 containing 0.1 M tetrabutylammonium hexafluorophosphate ($TBAPF_6$) at a scan rate of 100 mV s^{-1}.

from the first half-wave oxidation potential ($E^{ox}{}_{1/2}$). A similar behavior is observed for the four derivatives, showing three oxidation processes in the anodic region assigned to three consecutive one-electron oxidation processes, assigned to: i) the oxidation of both the arylamine units and the central fluorene to form a doublet cation, ii) the oxidation of the arylamine units leading to a singlet dication, and iii) the oxidation of the phenothiazine moiety to form a doublet trication (see Section S5, Supporting Information). The resulting HOMO and LUMO energies estimated for the new HTMs (shown in Figure 1b) ensure an effective hole transfer of the photogenerated holes from the valence band edge of the perovskite to the organic layer, leading to an optimal band alignment, potentially minimizing the voltage loss in the resultant devices.

2.2. Optoelectronic Characteristics of Perovskite Films with PTZ-Based HTMs

To further understand the impact of PTZ-based HTMs on the perovskite films, we examined both the time-resolved photoluminescence (TRPL) decays and steady-state PL quantum yields (PLQY) (**Figure** 3a,b; Figure S12, and Table S7, Supporting Information). Partial and full perovskite/HTM device stacks were fabricated to evaluate interface recombination and charge transfer. TRPL measurements on perovskite/HTM revealed that the perovskite with PTZ-Fl exhibited the fastest initial PL decay, which we attribute to rapid hole injection from the perovskite valence band to PTZ-F1. We systematically probed the PLQY and QFLS at three critical stages of the device formation: i) pristine perovskite films, ii) perovskite/HTM stacks, and iii) full perovskite/HTM/electrode devices. As shown in Figure 3a, introducing the PTZ-Fl hole-transport material (HTM) led to a substantial increase in PLQY for the partial stack (from 5.4% in the control to 11.3%), highlighting the strong effect of reduced interfacial defects and improved energy-level alignment at the perovskite/HTM interface. Notably, even upon deposition of the Au electrode, the PTZ-Fl–based device maintained a PLQY of 10.6%, indicating that the defect formation at the HTL/electrode interface was effectively minimized. Consistent with these observations, QFLS measurements revealed that PTZ-Fl introduced only a 58 mV difference from the pristine perovskite film to the full perovskite/HTM/electrode stack, underscoring minimal non-radiative recombination losses at the additional interfaces.

2.3. Photovoltaic Performance of the PSCs

We fabricated conventional PSCs using different PTZ-based HTMs with the planar structure of FTO/SnO_2-/perovskite/HTM/Au as shown in Figure 3c. Cross-sectional scanning electron spectroscopy (SEM) images show that the PTZ-based HTM films have a thinner thickness than the spiro-OMeTAD layer (Figure S13, Supporting Information). Figure 3d shows the current density-voltage (*J–V*) curves of the best PSCs for each given HTM under 1-sun irradiation at 100 mW cm^{-2} (detailed photovoltaic parameters are summarized in Table S8, Supporting Information). Notably, negligible hysteresis was observed in the *J–V* scans between forward and reverse sweeps in all devices with PTZ-based HTMs (Figure S14, Supporting Information). The control devices fabricated with spiro-OMeTAD as HTM exhibited a PCE of 23.08% with a short-circuit current (J_{SC}) of 25.13 mA cm^{-2}, an open-circuit voltage (V_{OC}) of 1.128 V, and a fill factor (FF) of 81.43%, consistent with a previous report.[30] Compared with control devices, the PSCs with PTZ-based HTMs demonstrated an overall performance improvement, attributed to the reduction in the non-radiative recombination rates between the perovskite film and the HTMs. Among these, the notably higher V_{OC} of the PTZ-Fl–based devices is explained by its deeper HOMO level, which ensures more favorable energy alignment with the perovskite valence band, and by its suppressed non-radiative recombination at both the perovskite/HTM and HTM/electrode interfaces, as supported by the PLQY and QFLS data (Figure 3b). Remarkably, devices with PTZ-Fl exhibited the best performance compared to the other PTZ-based HTMs, reaching the best PCE of 25.75% with J_{SC} of 26.14 mA cm^{-2}, V_{OC} of 1.177 V, and FF of 83.63%. A stabilized PCE of 25.4% was measured for a PSC with PTZ-Fl under maximum power point (MPP) tracking over a period of 300 s (Figure 3d, inset). Additionally, PTZ-3F achieved a PCE

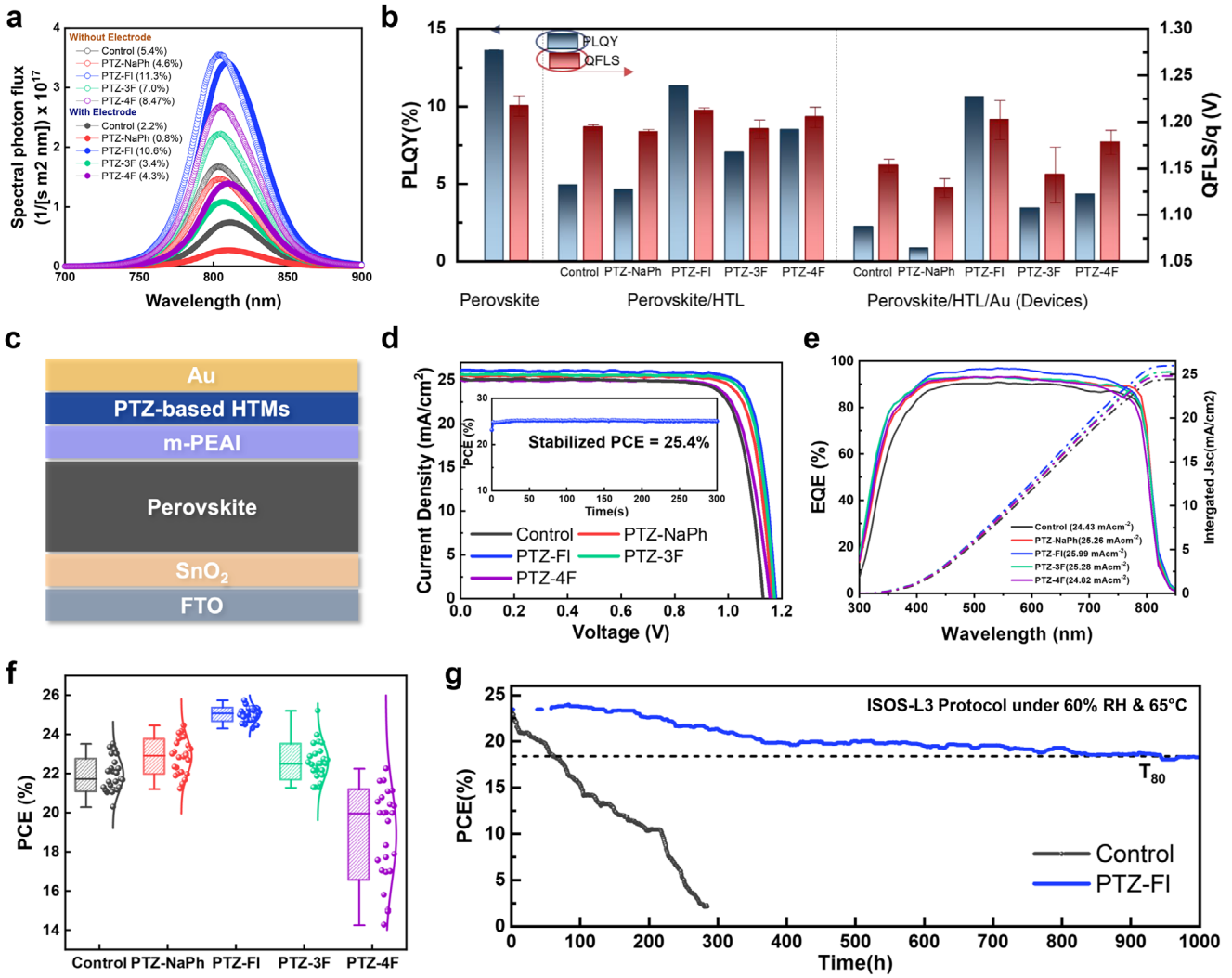

Figure 3. a) Absolute photoluminescence intensity and PLQY of perovskite devices. b) PLQY (left y axis) and QFLS (right y axis) for perovskite, perovskite/HTL, and perovskite/HTL/electrode. c) Device structure of planar PSCs. d) *J–V* curves of devices based on spiro-OMeTAD and PTZ-based HTMs, and stabilized output power of PSCs with PTZ-FI (inset). e) External quantum efficiency and integrated JSC of PSCs with HTMs. f) Statistical distribution of the PCEs obtained for 30 PSC devices based on spiro-OMeTAD and PTZ-based HTMs. g) Operational stability test of encapsulated PSCs with control (spiro-OMeTAD) and PTZ-FI, based on the ISOS L3 protocol.

exceeding 25%, while PTZ-NaPh reached 24.5%. PTZ-4F yielded a lower PCE of 23.18%, which may be attributed to a less uniform film formation (Figure S15, Supporting Information). Figure 3e shows the external quantum efficiency (EQE) spectra recorded for the PSCs. The integrated photocurrent densities match well with those shown in the *J–V* curves. Statistical analysis was also performed with 30 devices. The narrow PCE distribution of the PTZ-FI based PSCs indicates better reproducibility than for the spiro-OMeTAD-based PSCs (Figure 3f; Figure S16, Supporting Information). Encouraged by the excellent performance of the PSCs incorporating PTZ-based HTMs, the best PTZ-FI device was sent to an accredited laboratory (Newport, Irvine, CA, USA) for certification, where a stabilized PCE of 25.2% (with J_{SC} = 26.66 mA cm^{-2}, V_{OC} = 1.123 V and FF = 84.12% under the reverse bias) was obtained (Figure S18, Supporting Information).

The long-term stability tests of the encapsulated devices were conducted following the International Summit on Organic PV Stability (ISOS) protocol as shown in Figure 3g and Figures S19 and S20 (Supporting Information).[31] The shelf-life test, conducted in the dark at 25 °C with 30–60% relative humidity, showed that most of the PTZ HTMs retained an impressive 95% of their initial efficiency for 3600 h. Devices with PTZ-4F were the exception, with the PCE decreasing by > 30% over the same period. To further assess the operational stability, the ISOS-L3 testing protocol was carried out under continuous 1-sun irradiation at 65 °C and ≈60% relative humidity. Devices with PTZ-FI achieved a T_{80} of 1000 h after continuous maximum power point tracking, whereas control devices dropped from initial efficiency to below T_{80} within 80 h. To further assess thermal robustness, we performed cross-sectional SEM analysis after annealing fully assembled devices at 85 °C for 150 h. While spiro-OMeTAD

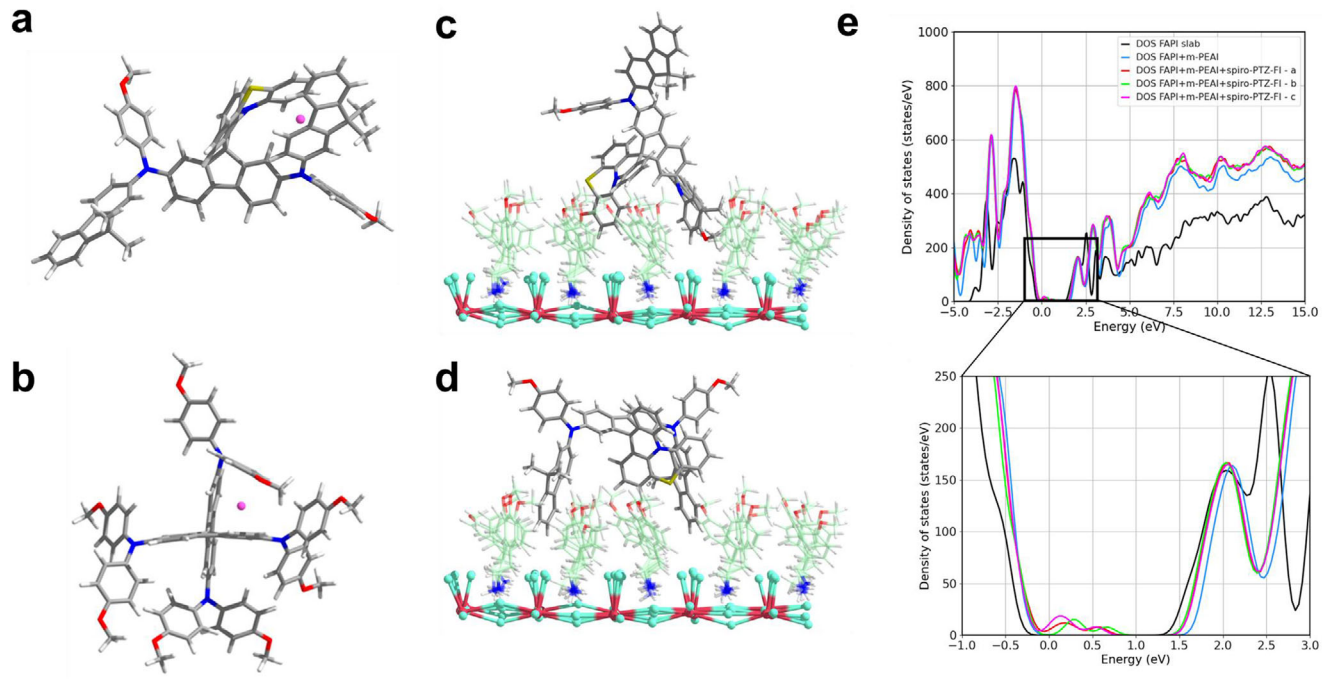

Figure 4. BMK/6-31G(d,p)-optimized Li^+ (pink color) binding modes of PTZ-Fl a) and spiro-OMeTAD b) with the largest association energy. c,d) PBEsol/tier-1 light NAO-optimized binding modes of PTZ-Fl to the m-PEAI passivated $FAPbI_3$ slab. m-PEAI cations are shown with high transparency and different colors to better show the degree of intercalation of the HTM. Color code for the HTM atoms: C (gray), S (yellow), N (blue), O (red), and H (white). Color code for the perovskite slab: Pb (dark red) and I (turquoise). The two underlying perovskite layers have been removed for simplicity. e) Density of states for the $FAPbI_3$ slab, the m-PEAI passivated perovskite and the m-PEAI passivated perovskite interacting with PTZ-Fl following the three binding modes shown in Figure S7 (Supporting Information).

films showed clear signs of morphological degradation—such as voids and delamination—PTZ-based HTMs, particularly PTZ-Fl, maintained smooth, uniform, and intact layers (Figure S21, Supporting Information). Complementing these morphological observations, we also carried out DSC in the presence of lithium bis(trifluoromethanesulfonyl)imide (LiTFSI) and *tert*-butylpyridine (*t*BP), as these additives are known to influence the T_g of HTMs (Figure S22, Supporting Information). Pristine spiro-OMeTAD exhibited a T_g of 125 °C, which upon doping drastically decreased to 62 °C.[32–34] In contrast, the T_g of dried-powder PTZ-Fl was determined to be 187 °C, which decreased to 153 °C upon the inclusion of LiTFSI and *t*BP. These results corroborate the superior thermal robustness of PTZ-Fl.

Additionally, PTZ-Fl demonstrates higher hydrophobicity in comparison with spiro-OMeTAD, as evidenced by the contact angle measurements (Figure S23, Supporting Information). The contact angles of doped PTZ-Fl and spiro-OMeTAD were measured to be 77.8 and 61.9, respectively, indicating significantly better moisture protection for PTZ-Fl.[35–37] This hydrophobicity contributes substantially to the improved stability of the PSCs based on the spiro-PTZ HTMs.

It has been reported that lithium cations migrate from the HTM into the perovskite layer, lowering the performance and the stability of the PSC.[38–41] We conducted time-of-flight secondary ion mass spectrometry (ToF-SIMS) depth profiling on aged PSCs after light irradiation. Figure S24 (Supporting Information) shows a significant reduction in Li^+ concentration in PTZ-Fl-based device compared to the control device. FTIR measurements were performed on LiTFSI, pristine HTMs, and HTMs doped with LiTFSI (Figure S24, Supporting Information). For the HTM with LiTFSI, the asymmetric vibration of the S-N-S central group in LiTFSI (1056 cm^{-1} for PTZ-Fl and 1053cm^{-1} for spiro-OMeTAD) was shifted to higher wavenumbers compared to pristine LiTFSI (1051 cm^{-1}), suggesting that the interaction between Li^+ and the $TFSI^-$ anion was weakened due to the affinity of Li^+ for the HTM.[32,42,43] Notably, the larger shift observed for PTZ-Fl denoted that stronger interactions are established in the case of PTZ-Fl than in spiro-OMeTAD, which retards the migration of Li^+ ions.

The greater Li^+ affinity of PTZ-Fl compared to spiro-OMeTAD was rationalized by means of theoretical calculations on HTM···Li^+ interacting dimers (see the Supporting Information for full details). Although the association energy calculated for the best interacting arrangements was similar for PTZ-Fl (–3.48 eV, **Figure** 4a) and spiro-OMeTAD (–3.56 eV, Figure 4b), the energy penalty required for PTZ-Fl to rearrange its minimum-energy structure toward Li^+ recognition was predicted significantly smaller (0.05 eV; Figure S5, Supporting Information) than that required for spiro-OMeTAD (0.18 eV; Figure S4, Supporting Information). Interestingly, PTZ-Fl effectively interacts with the Li^+ cation through an enveloping conformation, facilitated by the phenothiazine-fluorene embrace, which is expected to dynamically trap Li^+. Moreover, periodic DFT calculations performed on PTZ-Fl interacting with the m-PEAI-covered perovskite show that PTZ-Fl binds to the passivated surface by intercalation of the fluorene substituents and the phenothiazine core (Figure 4c,d; Figure

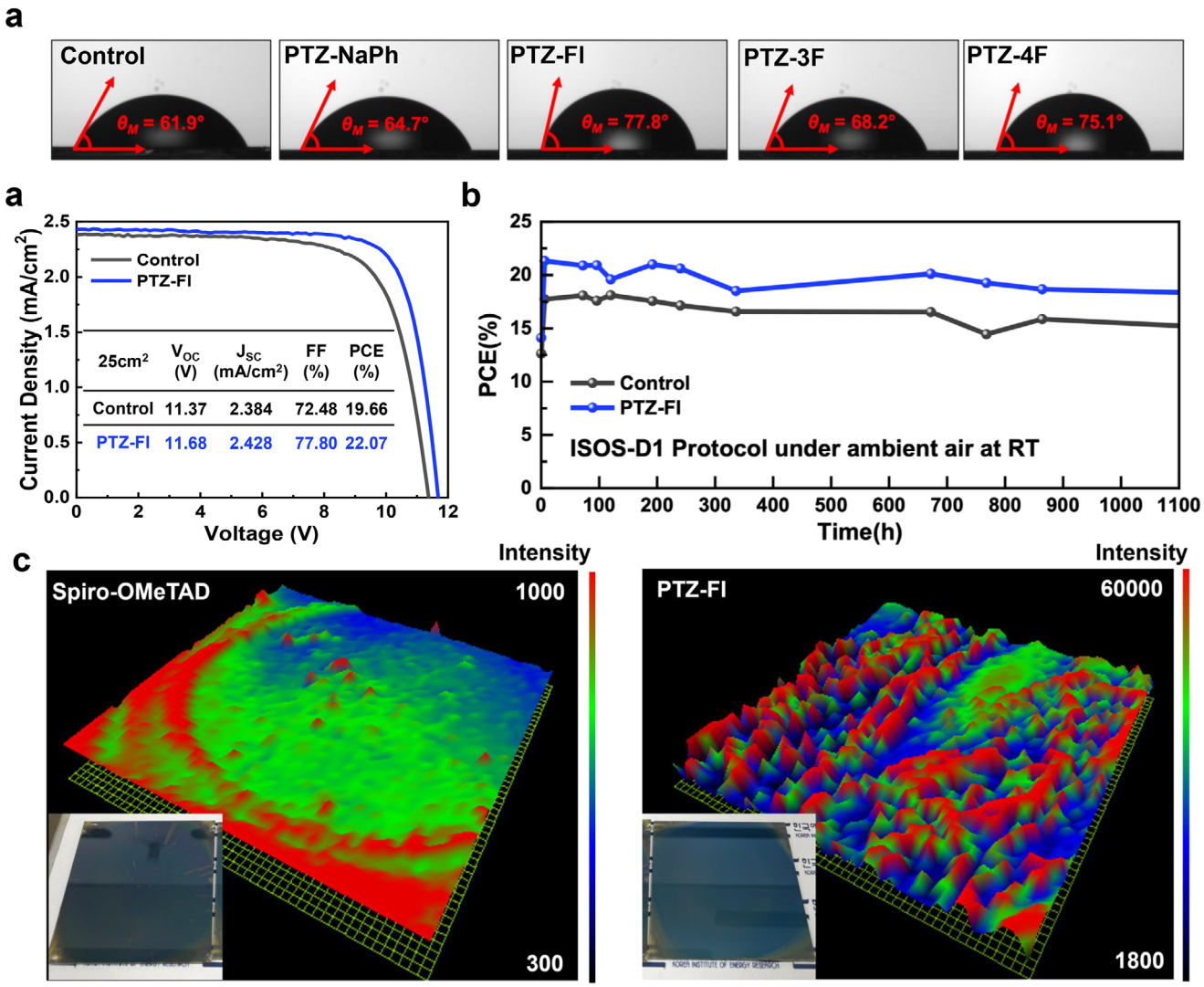

Figure 5. Characteristics of the perovskite mini-module with spiro-OMeTAD and PTZ-Fl. a) *J–V* curves. b) Shelf-life stability test under ISOS-D1 protocol. c) PL mapping image of large area (5 × 5 cm) perovskite films with control (left) and PTZ-Fl (right) and photograph of the perovskite films with control and PTZ-Fl (inset).

S7, Supporting Information). This intercalation gives rise to S···O contacts in the range of 3–5 Å between the positively charged S atom of the phenothiazine ring of the HTM and the negatively charged O atom of the terminal methoxy group of the passivating cations (Figure S8, Supporting Information). This compact interphase, which was not formed for spiro-OMeTAD, as it binds through the terminal benzene rings (Figure S6, Supporting Information), was expected to further retard the Li^+ migration in the PTZ-based PSCs. The hole extraction capability of PTZ-Fl was confirmed by the presence of HTM-centered electronic states within the perovskite bandgap (Figure 4e).

2.4. Performance and Stability of the Perovskite Mini Module

Achieving high efficiency in the manufacturing of large-area PSC modules has become crucial for their commercial deployment. In this regard, we successfully fabricated a PSC module with an active area of 25 cm^2. Given the high efficiency observed in small-area tests, we employed PTF-Fl as the hole-selective contact in the fabrication of the mini module. **Figure 5a** shows the *J–V* characteristics and images of the perovskite module with PTZ-Fl, which achieved a PCE of 22.07% with J_{SC} of 2.428 mA cm^{-2}, V_{OC} of 11.68 V, and FF of 77.8%. PL mapping of the large-area perovskite film (Figure 5c) revealed substantial differences in the PL intensity between the spiro-OMeTAD and PTZ-Fl coated films. Additionally, a 36 cm^2 substrate was divided into nine sections and the roughness of the film on each section was measured using atomic force microscopy (AFM) (Figures S26 and S27, Supporting Information). The control film had an average root mean square (RMS) roughness of 17.82, while the PTZ-Fl film exhibited a slightly higher RMS value of 19.35. However, the PTZ-Fl film showed a much smaller RMS deviation of 1.25, compared to 3.30 for the control, indicating a more uniform film formation.

Moreover, pinholes were observed in the control film, which is consistent with the device performance of the control perovskite module. Additionally, the operational stability test was conducted under ambient air at room temperature (Figure 5b). The mini module with PTZ-Fl retained 85% of its initial efficiency after 1100 h under the ISOS-D1 test protocol, demonstrating that the PTZ-based HTMs also show strong potential for the efficient, stable, and scalable production of PSC modules.

3. Conclusion

In summary, tailored chemical modification of peripheral arylamines into the spiro-phenothiazine-based central core (PTZ) allowed the preparation of four new and efficient organic (HTMs). The novel spiro-PTZ-based HTMs have been tested in the fabrication of n-i-p PSCs, yielding outstanding PCE values surpassing 23%. Notably, PTZ-Fl, bearing dimethylfluorene in the periphery, showed an impressive maximum PCE of 25.75% (25.2% certified), outperforming reference cells including benchmark spiro-OMeTAD. Furthermore, remarkable stability following ISOS protocols has been proved, showing that PTZ-Fl retains 95% of PCE under ISOS-D1 (over 3600 h) and displays a T_{80} of 1000 h in ISOS-L3 (in sharp contrast to spiro-OMeTAD, showing a T_{80} within 80 h). The enhanced stability is explained by different approaches. ToF-SIMS and FTIR measurements showed that PTZ-Fl presents a significant reduction in Li^+ concentration within the perovskite layer, typically attributed to triggering its decomposition. DFT theoretical calculations predicted that PTZ-Fl has a larger Li^+ affinity and can be efficiently intercalated into the m-PEAI passivation layer, giving rise to a compact interphase that contributes to reducing Li^+ migration. Enhanced thermal stability can be attributed to the improved T_g under doped conditions shown by PTZ-Fl (153 °C). Additionally, minimodules of 25 cm^2 area have been fabricated, reaching efficiencies over 22% (notably higher than that shown by spiro-OMeTAD), also demonstrating an improved stability under ISOS-D1 protocol. Gathering all the results, the use of the simple spiro-PTZ core is demonstrated as an excellent backbone for the preparation of efficient and stable hole-transporting materials. Particularly, PTZ-Fl reached one of the highest PCEs reported in the bibliography (for non-commercially available materials), highlighting also in its stability and efficiency in large-scale PSC devices.

Supporting Information

Supporting Information is available from the Wiley Online Library or from the author.

Acknowledgements

The authors thank UCRF (UNIST Central Research Facilities) for support of using the equipment. This research was supported by Learning & Academic research institution for Master's·PhD students, and Postdocs (LAMP) Program of the National Research Foundation of Korea (NRF) grant funded by the Ministry of Education (RS-2023-00301974). Y.J. gratefully acknowledges the Technology Development Program to Solve Climate Changes of the National Research Foundation (NRF), funded by the Ministry of Science, ICT & Future Planning (2020M1A2A2080746) and the Development Program of the Korea Institute of Energy Research (KIER) (C4-2414 and C4-2460). J.J., L.Z., S.M.Z. and M.G. acknowledge financial support from the Güneş Perovskite Solar Cell A.S. company, Adana, Turkey and European Union's Horizon 2020 research and innovation program under grant 881603. N.M., A.M.-O. and J. U.-M. thanks financial support to MCIN/AEI of Spain (projects PID2020-114653RB-I00, and TED2021-131255B-C44 funded by MCIN/AEI/10.13039/501100011033 and "(MAD2D-CM)-UCM" projects funded by Comunidad de Madrid, by the Recovery, Transformation and Resilience Plan, and by NextGenerationEU from the European Union. E.O. and J.C. also acknowledge the MICIN/AEI of Spain (projects PID2021-128569NB-I00, PID2020-119748GA-I00, TED2021-131255B-C44 and RED2022-134939-T funded by MCIN/AEI/10.13039/501100011033 and by "ERDF A way of making Europe") and the Generalitat Valenciana (Grant No. MFA/2022/017). Project MFA/2022/017 forms part of the Advanced Materials program supported by MCIN with funding from European Union NextGenerationEU (PRTR-C17.I1) and by Generalitat Valenciana. A.M.-O. is grateful to MCIN for a "Ramon-y-Cajal" fellowship (RYC2019-027939-I). M.P.-E. acknowledges the PRE2021-097082 grant funded by MCIN/AEI and "ESF Investing in your future".

Conflict of Interest

The authors declare no conflict of interest.

Author Contributions

J.U.-M., S.C., M.P-E, and J.J. contributed equally to this work. A.M.-O., Y.J., N.M, E.O, J.C., and M.G. designed and supervised the project. A.M.-O., S.-Y.Y., and S.M.Z advised on the research. J.U.-M., S.O., A.M.-O., and I.G.-B. synthesized and characterized organic materials. S.C. and J.J. developed the concept and analyzed experimental data. L.Z. performed PLQY measurements. S.S. measured GIWAXS and ToF-SIMs. M.B. characterized the perovskite film with TRPL. M. P.-E. performed the theoretical calculations. J.U.-M, M.P.-E., J.J., and A.M.-O. wrote the manuscript. J.C., M.P.-E., and E.O. revised and edited the manuscript. All the authors contributed to the discussion of the manuscript.

Data Availability Statement

The data that support the findings of this study are available from the corresponding author upon reasonable request.

Keywords

hole transporting materials, perovskite solar cells, power conversion efficiency

Received: March 21, 2025
Revised: June 17, 2025
Published online:

[1] A. Kojima, K. Teshima, Y. Shirai, T. Miyasaka, *J. Am. Chem. Soc.* **2009**, *131*, 6050.
[2] N. R. E. L. National Renewable Energy Laboratory, https://www.nrel.gov/pv/cell-efficiency, (accessed: July 2025).
[3] C. Liu, Y. Yang, H. Chen, J. Xu, A. Liu, A. S. R. Bati, H. Zhu, L. Grater, S. S. Hadke, C. Huang, V. K. Sangwan, T. Cai, D. Shin, L. X. Chen, M. C. Hersam, C. A. Mirkin, B. Chen, M. G. Kanatzidis, E. H. Sargent, *Science* **2023**, *382*, 810.

[4] M. Kim, J. Jeong, H. Lu, T. K. Lee, F. T. Eickemeyer, Y. Liu, I. W. Choi, S. J. Choi, Y. Jo, H.-B. Kim, S.-I. Mo, Y.-K. Kim, H. Lee, N. G. An, S. Cho, W. R. Tress, S. M. Zakeeruddin, A. Hagfeldt, J. Y. Kim, M. Grätzel, D. S. Kim, *Science* **2022**, *375*, 302.
[5] Y. Shen, T. Zhang, G. Xu, J. A. Steele, X. Chen, W. Chen, G. Zheng, J. Li, B. Guo, H. Yang, Y. Wu, X. Lin, T. Alshahrani, W. Yin, J. Zhu, F. Wang, A. Amassian, X. Gao, X. Zhang, F. Gao, Y. Li, Y. Li, *Nature* **2024**, *635*, 882.
[6] J. Jeong, M. Kim, J. Seo, H. Lu, P. Ahlawat, A. Mishra, Y. Yang, M. A. Hope, F. T. Eickemeyer, M. Kim, Y. J. Yoon, I. W. Choi, B. P. Darwich, S. J. Choi, Y. Jo, J. H. Lee, B. Walker, S. M. Zakeeruddin, L. Emsley, U. Rothlisberger, A. Hagfeldt, D. S. Kim, M. Grätzel, J. Y. Kim, *Nature* **2021**, *592*, 381.
[7] S. Li, Y. Jiang, J. Xu, D. Wang, Z. Ding, T. Zhu, B. Chen, Y. Yang, M. Wei, R. Guo, Y. Hou, Y. Chen, C. Sun, K. Wei, S. M. H. Qaid, H. Lu, H. Tan, D. Di, J. Chen, M. Grätzel, E. H. Sargent, M. Yuan, *Nature* **2024**, *635*, 82.
[8] S. Chen, N. Liu, F. Xu, G. Wei, *Sol. RRL* **2023**, *7*, 2300479.
[9] B. Chen, P. N. Rudd, S. Yang, Y. Yuan, J. Huang, *Chem. Soc. Rev.* **2019**, *48*, 3842.
[10] Y. Li, H. Wu, W. Qi, X. Zhou, J. Li, J. Cheng, Y. Zhao, Y. Li, X. Zhang, *Nano Energy* **2020**, *77*, 105237.
[11] C. C. Boyd, R. Cheacharoen, T. Leijtens, M. D. McGehee, *Chem. Rev.* **2019**, *119*, 3418.
[12] S. Sajid, S. Alzahmi, I. Ben Salem, J. Park, I. M. Obaidat, *Mater. Today Energy* **2023**, *37*, 101378.
[13] C. Zhang, X. Shen, M. Chen, Y. Zhao, X. Lin, Z. Qin, Y. Wang, L. Han, *Adv. Energy Mater.* **2023**, *13*, 2203250.
[14] Q. Fu, X. Tang, H. Liu, R. Wang, T. Liu, Z. Wu, H. Y. Woo, T. Zhou, X. Wan, Y. Chen, Y. Liu, *J. Am. Chem. Soc.* **2022**, *144*, 9500.
[15] Y. Bai, Z. Zhou, Q. Xue, C. Liu, N. Li, H. Tang, J. Zhang, X. Xia, J. Zhang, X. Lu, C. J. Brabec, F. Huang, *Adv. Mater.* **2022**, *34*, 2110587.
[16] J. Urieta-Mora, I. García-Benito, A. Molina-Ontoria, N. Martín, *Chem. Soc. Rev.* **2018**, *47*, 8541.
[17] P. Yan, D. Yang, H. Wang, S. Yang, Z. Ge, *Energy Environ. Sci.* **2022**, *15*, 3630.
[18] W. S. Yang, B. W. Park, E. H. Jung, N. J. Jeon, Y. C. Kim, D. U. Lee, S. S. Shin, J. Seo, E. K. Kim, J. H. Noh, S. Il Seok, *Science* **2017**, *356*, 1376.
[19] M. Jeong, I. W. Choi, E. M. Go, Y. Cho, M. Kim, B. Lee, S. Jeong, Y. Jo, H. W. Choi, J. Lee, J.-H. Bae, S. K. Kwak, D. S. Kim, C. Yang, *Science* **2020**, *369*, 1615.
[20] M. Jeong, I. W. Choi, K. Yim, S. Jeong, M. Kim, S. J. Choi, Y. Cho, J.-H. An, H.-B. Kim, Y. Jo, S.-H. Kang, J.-H. Bae, C.-W. Lee, D. S. Kim, C. Yang, *Nat. Photonics* **2022**, *16*, 119.
[21] J. Urieta-Mora, I. García-Benito, L. A. Illicachi, J. Calbo, J. Aragó, A. Molina-Ontoria, E. Ortí, N. Martín, M. K. Nazeeruddin, *Sol. RRL* **2021**, *5*, 2100650.
[22] A. Molina-Ontoria, I. Zimmermann, I. Garcia-Benito, P. Gratia, C. Roldán-Carmona, S. Aghazada, M. Graetzel, M. K. Nazeeruddin, N. Martín, *Angew. Chem., Int. Ed.* **2016**, *55*, 6270.
[23] I. García-Benito, I. Zimmermann, J. Urieta-Mora, J. Aragó, J. Calbo, J. Perles, A. Serrano, A. Molina-Ontoria, E. Ortí, N. Martín, M. K. Nazeeruddin, *Adv. Funct. Mater.* **2018**, *28*, 1801734.
[24] J. Xia, P. Luizys, M. Daskeviciene, C. Xiao, K. Kantminiene, V. Jankauskas, K. Rakstys, G. Kreiza, X.-X. Gao, H. Kanda, K. G. Brooks, I. R. Alwani, Q. U. Ain, J. Zou, G. Shao, R. Hu, Z. Qiu, A. Slonopas, A. M. Asiri, Y. Zhang, P. J. Dyson, V. Getautis, M. K. Nazeeruddin, *Adv. Mater.* **2023**, *35*, 2300720.
[25] Y. Wei, Y. Cai, L. He, Y. Zhang, Y. Yuan, J. Zhang, P. Wang, *Chem. Sci.* **2023**, *14*, 10285.
[26] M. Caicedo-Reina, M. Pérez-Escribano, J. Urieta-Mora, I. García-Benito, J. Calbo, A. Ortiz, B. Insuasty, A. Molina-Ontoria, E. Ortí, N. Martín, *J. Mater. Chem. C* **2023**, *11*, 8223.
[27] H. Zhang, X. Yu, M. Li, Z. Zhang, Z. Song, X. Zong, G. Duan, W. Zhang, C. Chen, W.-H. Zhang, Y. Liu, M. Liang, *Angew. Chem., Int. Ed.* **2023**, *62*, 202314270.
[28] K. Yang, Q. Liao, J. Huang, Z. Zhang, M. Su, Z. Chen, Z. Wu, D. Wang, Z. Lai, H. Y. Woo, Y. Cao, P. Gao, X. Guo, *Angew. Chem., Int. Ed.* **2022**, *61*, 202113749.
[29] X. Ji, T. Zhou, Q. Fu, W. Wang, Z. Wu, M. Zhang, X. Guo, D. Liu, H. Y. Woo, Y. Liu, *Adv. Energy Mater.* **2023**, *13*, 2203756.
[30] Q. Jiang, Y. Zhao, X. Zhang, X. Yang, Y. Chen, Z. Chu, Q. Ye, X. Li, Z. Yin, J. You, *Nat. Photonics* **2019**, *13*, 460.
[31] M. V Khenkin, E. A. Katz, A. Abate, G. Bardizza, J. J. Berry, C. Brabec, F. Brunetti, V. Bulović, Q. Burlingame, A. Di Carlo, R. Cheacharoen, Y.-B. Cheng, A. Colsmann, S. Cros, K. Domanski, M. Dusza, C. J. Fell, S. R. Forrest, Y. Galagan, D. Di Girolamo, M. Grätzel, A. Hagfeldt, E. von Hauff, H. Hoppe, J. Kettle, H. Köbler, M. S. Leite, S. Liu, Y.-L. Loo, J. M. Luther, et al., *Nat. Energy* **2020**, *5*, 35.
[32] S.-G. Kim, T. H. Le, T. de Monfreid, F. Goubard, T.-T. Bui, N.-G. Park, *Adv. Mater.* **2021**, *33*, 2007431.
[33] N. J. Jeon, H. Na, E. H. Jung, T.-Y. Yang, Y. G. Lee, G. Kim, H.-W. Shin, S. Il Seok, J. Lee, J. Seo, *Nat. Energy* **2018**, *3*, 682.
[34] T. Malinauskas, D. Tomkute-Luksiene, R. Sens, M. Daskeviciene, R. Send, H. Wonneberger, V. Jankauskas, I. Bruder, V. Getautis, *ACS Appl. Mater. Interfaces* **2015**, *7*, 11107.
[35] J. Jeong, T. Chawanpunyawat, M. Kim, V. Sláma, N. Lempesis, L. Agosta, V. Carnevali, Q. Zhang, F. T. Eickemeyer, L. Pfeifer, Y. Kim, J. W. Song, H. Lu, M. Almalki, S.-I. Mo, S. M. Zakeerudin, U. Rothlisberger, D. S. Kim, P. J. Dyson, M. Grätzel, *Adv. Energy Mater.* **2025**, *15*, 2401965.
[36] H. Kim, S.-U. Lee, D. Y. Lee, M. J. Paik, H. Na, J. Lee, S. Il Seok, *Adv. Energy Mater.* **2019**, *9*, 1902740.
[37] R. Azmi, S. Zhumagali, H. Bristow, S. Zhang, A. Yazmaciyan, A. R. Pininti, D. S. Utomo, A. S. Subbiah, S. De Wolf, *Adv. Mater.* **2024**, *36*, 2211317.
[38] Z. Li, C. Xiao, Y. Yang, S. P. Harvey, D. H. Kim, J. A. Christians, M. Yang, P. Schulz, S. U. Nanayakkara, C.-S. Jiang, J. M. Luther, J. J. Berry, M. C. Beard, M. M. Al-Jassim, K. Zhu, *Energy Environ. Sci.* **2017**, *10*, 1234.
[39] J. Kong, Y. Shin, J. A. Röhr, H. Wang, J. Meng, Y. Wu, A. Katzenberg, G. Kim, D. Y. Kim, T.-D. Li, E. Chau, F. Antonio, T. Siboonruang, S. Kwon, K. Lee, J. R. Kim, M. A. Modestino, H. Wang, A. D. Taylor, *Nature* **2021**, *594*, 51.
[40] X. Liu, B. Zheng, L. Shi, S. Zhou, J. Xu, Z. Liu, J. S. Yun, E. Choi, M. Zhang, Y. Lv, W.-H. Zhang, J. Huang, C. Li, K. Sun, J. Seidel, M. He, J. Peng, X. Hao, M. Green, *Nat. Photonics* **2023**, *17*, 96.
[41] J. A. Dawson, A. J. Naylor, C. Eames, M. Roberts, W. Zhang, H. J. Snaith, P. G. Bruce, M. S. Islam, *ACS Energy Lett.* **2017**, *2*, 1818.
[42] H. Qiu, X. Du, J. Zhao, Y. Wang, J. Ju, Z. Chen, Z. Hu, D. Yan, X. Zhou, G. Cui, *Nat. Commun.* **2019**, *10*, 5374.
[43] K. P Reddy, P. Fischer, M. Marinaro, M. Wohlfahrt-Mehrens, *ChemElectroChem* **2018**, *5*, 2758.